HHS Public Access

Author manuscript

Nature. Author manuscript; available in PMC 2018 July 10.

Published in final edited form as:

Nature. 2018 January 10; 553(7687): 165–170. doi:10.1038/nature25192.

Neurexin controls plasticity of a mature, sexually dimorphic neuron

Michael P. Hart and **Oliver Hobert**

Department of Biological Sciences, Howard Hughes Medical Institute, Columbia University, New York, NY, USA

Abstract

During development and adulthood, brain plasticity is evident at several levels, from synaptic structure and function to outgrowth of dendrites and axons. Whether and how sex impinges on neuronal plasticity is poorly understood. Here we show that the *C. elegans* sex-shared GABAergic DVB neuron displays experience-dependent and sexually dimorphic morphologic plasticity, characterized by the stochastic and dynamic addition of multiple neurites in adult males. These added neurites enable synaptic rewiring of the DVB neuron, instructing a functional switch of the neuron and directly modifying a step of male mating behavior, both of which are altered by experience and post-synaptic activity manipulations. We show that the outgrowth of DVB neurites is promoted by presynaptic NRX-1/neurexin and restricted by postsynaptic NLG-1/neuroligin, providing a novel context in which these two molecules operate.

Experience modifies the structure and function of neurons and circuits in the brain through multiple mechanisms of neuronal plasticity[1,2]. Plasticity in adulthood refines circuits in response to experience for adaptation, homeostasis, and as a cellular correlate of learning and memory[1,3,4], including extension and retraction of dendrites and axons[5–7]. The molecular mechanisms underlying this morphological plasticity in adult neurons are not well understood. Similarly, while sexual identity of an organism impacts nervous system function and plasticity, the molecular and cellular basis of such sexual dimorphisms are also not fully understood.

Morphologic plasticity displayed by adult male DVB neuron

The GABAergic motor/inter-neuron DVB is located in the tail of *C. elegans* and projects its process anteriorly in the ventral nerve cord in both sexes (Fig. 1a). Visualizing DVB with fluorescent r eporter gene technology, we found that DVB displays extensive post-developmental morphologic plasticity exclusively in male animals, characterized by the

Correspondence to: Oliver Hobert (or38@columbia.edu).

Author Contributions

M.P.H. and O.H. designed the experiments and wrote the manuscript. M.P.H. performed the experiments.

Author Information

The authors declare no conflicts of interest.

progressive extension of new neurites posteriorly into the tail (Fig. 1b; Extended Data Fig. 1). The total neurite length and the number of neurite junctions significantly increase from day 1 to day 5 of adult life (Fig. 1c,d). The branching pattern of male DVB neurites lacks any overt stereotypy (Extended Data Fig. 2a,b). The generation of new DVB neurites in males is accompanied by the addition of presynaptic, RAB-3(+) boutons suggesting these neurites represent axon-like projections (Fig. 1b, Extended Data Fig. 1) and is corroborated by EM analysis[8,9]. We have not identified other neurons that undergo comparable neurite outgrowth in adulthood (Fig. 1b, Extended Data Fig. 2c–h).

DVB plasticity impacts behavior via dimorphic synaptic connectivity

In hermaphrodites, DVB controls defecation behavior[10], while in males DVB also contributes to protraction of the male-specific spicule structures, which are inserted into the hermaphrodite vulva during copulation (Fig. 1e–g)[11]. Consistent with a sexually dimorphic function, the synaptic wiring pattern of DVB is also strikingly sexually dimorphic (Fig. 1g)[8,9]. To test for functional roles of DVB neurite outgrowth, we examined DVB function over the period of DVB neurite outgrowth. Day 1 males were previously found to protract their spicules briefly following the expulsion step of defecation due to connections between defecation and spicule circuits[11]. This seemingly pointless protraction can result in chronic protraction of spicules, which is detrimental to male mating ability. We found that day 1, but not day 3 males, frequently protract spicules during expulsion (Extended Data Fig. 3b)[12]. To determine any role for DVB in this change, we silenced DVB using expression of a histamine-gated chloride channel (*lim-6*^{int4}*::HisCl1* with histamine), which resulted in increased protraction of spicules with expulsion at day 3 (Extended Data Fig. 3b). The time between consecutive expulsions was unchanged in day 1 to day 3 in controls, but slightly increased in DVB-silenced day 3 males (Extended Data Fig. 3c). These results suggest that DVB plays a role in reducing expulsion-associated spicule protraction during the period of neurite outgrowth, likely through inhibition of spicule circuit components that connect with the defecation circuit. Moreover, laser ablation of DVB in day 1 males (Extended Data Fig. 3d) resulted in a reduction in the number of males with chronically protracted spicules compared to controls, whereas ablation of DVB at each day after day 2 resulted in a progressive increase in animals with chronically protracted spicules (Fig. 2a). This demonstrates that DVB contributes to spicule protraction at day 1, and confirms that DVB functions to inhibit spicule protraction after day 2, with a functional consequence of suppressing spicule protraction during expulsion.

We validated these findings using expression of channelrhodopsin in DVB (Extended Data Fig. 3e). Light-induced activation of DVB in day 1 adult males resulted in observable movement of spicules, whereas activation of DVB at day 5 resulted in only rare movement of spicules (Fig. 2b, Video 1). Channelrhodopsin expression and activation in the spicule protraction neurons and muscles always resulted in spicule protraction at days 1 and 5 (Fig. 2b, Video 2, Extended Data Fig. 3f). The fraction of male animals exhibiting spicule movement after channelrhodopsin-mediated DVB activation at day 1 was unchanged in males lacking GABA signaling components (*unc-25*/GAD or *unc-49*/$GABA_A$ receptor mutants)(Fig. 2c). indicating that DVB may signal through electrical connections and/or neuropeptide signaling[11]. While DVB neurite outgrowth is not affected in *unc-49* mutants,

these animals did show a reduction in spicule protraction at day 5 (aldicarb assay described below, Extended Data Fig. 4a–d), suggesting that GABA contributes to restriction of spicule protraction in later adulthood.

To further characterize the role of DVB in active spicule protraction, we utilized the acetylcholine esterase inhibitor, aldicarb, which results in spicule protraction through the accumulation of acetylcholine at neuromuscular synapses onto spicule protractor muscles (Fig. 2d)[13]. We found that aldicarb-induced spicule protraction takes longer as males age from day 1 to day 5 (Fig. 2e), during the same period as DVB neurite outgrowth. To directly establish any role for DVB in this behavioral change, we combined laser ablation of DVB with aldicarb-induced spicule protraction. DVB ablation at day 1 resulted in slower spicule protraction in response to aldicarb than in control and mock-ablated males, again demonstrating that DVB input at day 1 has an excitatory effect on spicule protraction (Fig. 2f). DVB ablation at day 5 resulted in faster spicule protraction in response to aldicarb than in control and mock-ablated males, demonstrating a functional switch for DVB from an excitatory to an inhibitory input on spicule protraction by day 5 (Fig. 2f). These results were confirmed using genetic ‘ablation’ of DVB (*lim-6* transcription factor mutant[14])(Fig. 2f). Taken together, our results confirm that DVB switches function in adulthood, and implicate DVB as the main contributor to the temporal change observed in spicule protraction and defecation behavior.

How does the switch of DVB function during DVB neurite outgrowth relate to changes in synaptic connectivity? We used trans-synaptic labeling (GRASP[15]) to visualize synapses between DVB and the spicule protraction neurons and muscles (Fig. 2g). We found the number of these specific synaptic connections to increase from day 1 to 5 (Fig. 2h–i). We also visualized synapses between DVB and the spicule retractor muscles (Fig. 2j; Extended Data Fig. 4h) and found the number of these synapses to decrease from day 1 to 5 (Fig. 2k–l). These results provide evidence that structural remodeling of axons and dendrites in adulthood can rewire specific synaptic targets, supporting the notion that this remodeling can drastically alter connectivity within circuits and impact downstream behavior.

Male spicule protraction into the hermaphrodite vulva is the most complex step of the male mating behavior involving coordination of cholinergic and GABAergic signaling[16–18]. The balance of excitatory and inhibitory signaling is crucial for successful spicule insertion, which must be further coordinated with sex muscle excitability changes in early adulthood[13,19–21]. Day 1 and day 3 males are proficient at most steps of mating[20], however, in 5-minute timed mating assays, day 3 males were significantly more likely to successfully complete mating with sperm transfer (Extended Data Fig. 5a). Scoring the spicule-related steps of mating (spicule prodding and spicule protraction) demonstrated that day 1 males show more spicule prodding attempts overall and a lower ratio of protraction/prodding attempts compared with day 3 males (Extended Data Fig. 5b,c), indicating day 1 males are less capable of transitioning from spicule prodding to spicule protraction than day 3 males. This suggests that the morphologic and functional plasticity of DVB in males may fine-tune and coordinate the defecation and spicule protraction circuits to increase mating success.

DVB neurites are experience and activity-dependent

To determine if DVB plasticity is responding to experience, we tested if the act of mating itself alters DVB neuron morphology by exposing males to hermaphrodites for the first 48 hours of adulthood. Single males housed with hermaphrodites showed significant increases in DVB neurite length and junctions compared to males housed alone (Fig. 3a–c). *C. elegans* males housed with other males or in isolation can engage in mating-like behaviors, which may include spicule protraction. To minimize mating sensory input and self-mating behavior, we analyzed DVB neurite outgrowth in *pkd-2*/PKD2 mutant males[22] and in genetically paralyzed males (*unc-97*)[23]. *pkd-2* mutant males have reduced DVB neurite outgrowth at day 3 while genetically paralyzed males have almost no DVB neurites at day 3 (Extended Data Fig. 4e–g), but can protract spicules in response to aldicarb (data not shown) and neurites can be ectopically induced (Extended Data Fig. 5d–f). Paralyzed males also show no change in neurite outgrowth when housed with hermaphrodites for 48 hours (Fig. 3a–c). These results demonstrate that DVB neurite outgrowth is experience-dependent, potentially driven by spicule protraction and activity of the post-synaptic spicule protraction circuit.

Does activity of the post-synaptic targets of DVB contribute to DVB neurite outgrowth? Channelrhodopsin-mediated activation of post-synaptic DVB targets (spicule neurons and muscle) resulted in the immediate protraction of the spicules (Fig. 2b, Video 2)[16]. Repeated activation of the spicule protraction circuit caused a significant increase in DVB neurites (Fig. 3d–f, day 1), independent of GABA signaling (Extended Data Fig. 5d–f). Males exposed to repeated activation, but subsequently allowed to recover, had DVB neurites indistinguishable from controls, suggesting neurite growth is dynamic and potentially reversible (Fig. 3d–f). Repeated activation of either spicule neurons or muscles separately, demonstrated that activity in either can induce DVB neurite growth (Extended Data Fig. 5g–i). We next asked if activity-induced DVB neurites impact DVB neuron function and animal behavior. We activated and recovered males in the same manner as above, and then used the aldicarb assay to analyze spicule protraction behavior. Males at day 1 following repeated activation of the spicule protraction circuit showed a significant delay in the time to aldicarb-induced protraction (Fig. 3g, day 1), implying that activity-induced neurites have a direct and immediate effect on DVB spicule function. Males exposed to repeated activation of the spicule protraction circuit, but allowed to recover, had spicule protraction indistinguishable from day 2 controls (Fig. 3g, day 2), indicating that induced behavioral changes are dynamic and repeated activation does not result in lasting protraction defects.

To test if reducing circuit activity impacts DVB neurites, we exposed males to exogenous GABA, expecting to silence the targets of GABAergic DVB. This indeed resulted in a reduction of DVB neurites (Extended Data Fig. 6a–c). To implicate spicule circuit inhibition more specifically, we silenced spicule protraction neurons and muscles with a histamine-gated chloride channel in day 5 males, which also reduced DVB neurites (Extended Data Fig. 6d–f). In summary, DVB neurites grow out in response to activity levels of the spicule protraction circuit, including post-synaptic targets of DVB.

Neurexin and neuroligin control DVB plasticity

DVB neurite outgrowth appears to be a form of morphological and functional plasticity that fine-tunes the excitatory and inhibitory balance for coordinated spicule protraction. Many synaptic molecules are implicated in excitatory and inhibitory balance, including the synaptic adhesion molecules neurexin and its trans-synaptic binding partner neuroligin[24–27]. Examining neuroligin and neurexin for roles in controlling DVB neurite outgrowth, we find that males with a deletion allele of the single *C. elegans* neuroligin ortholog, *nlg-1,* display increased DVB neurite outgrowth at day 3 compared to controls (Fig. 4a–c). The increase in DVB neurite outgrowth at day 3 was rescued with a GFP-tagged NLG-1 expressed under its own promoter (Extended Data Fig. 7a–c), which is localized in a punctate pattern in numerous neurons and muscles of the male tail (Extended Data Fig. 8). *nlg-1* mutants displayed a spicule protraction phenotype which matches the expected phenotypes observed upon increasing DVB branching (Fig. 4d). *nlg-1* expression in DVB, SPC/PCA/PCB, or SPC/spicule muscles did not rescue the *nlg-1* mutant phenotype, whereas expression in the spicule protractor and anal depressor muscles or in the spicule retractor muscles did rescue (Extended Data Fig. 7d–e), indicating that NLG-1 contributes to DVB neurite outgrowth by functioning in multiple post-synaptic DVB muscles. Silencing the spicule protraction circuit in *nlg-1* mutant males at day 5 with *gar-3b::HisCl1* or overnight exposure to exogenous GABA resulted in no significant reduction in DVB neurite branching (Extended Data Fig. 7f–g). These results suggest that the *nlg-1* mutant phenotype cannot be explained by indirect alteration of the spicule circuit or more global perturbations in activity as a result of loss of NLG-1.

Unexpectedly, males with a deletion allele of *nrx-1*/neurexin[28] displayed a significant reduction in neurite outgrowth at day 3 and 5, a phenotype opposite to the *nlg-1* mutant phenotype (Fig. 4e–g). *nrx-1* mutants display a corresponding decrease in time to aldicarb-induced spicule protraction (Fig. 4h). The *nrx-1* locus produces both a long and short isoform[29] and two long isoform-specific mutant alleles recapitulated the null phenotype (Extended Data Fig. 9a–c). Repeated channelrhodopsin-mediated activation of the spicule protraction circuit failed to induce DVB neurites in *nrx-1* mutants (Extended Data Fig. 5d–f), indicating that the *nrx-1* phenotype is not explained solely by reduced circuit activity that could result from NRX-1 loss.

NRX-1 is broadly expressed throughout the *C. elegans* nervous system[29]. Expression of the long isoform of NRX-1 in DVB using the *lim-6*^{int4} promoter resulted in rescue of the *nrx-1(wy778)* neurite outgrowth defect (Extended Data Fig. 9d,e). The long NRX-1 isoform still rescued the mutant phenotype even after deletion of the C-terminal PDZ binding domain, while the short NRX-1 isoform did not (Extended Data Fig. 9d,e). Overexpression of the long isoform of NRX-1 in wildtype male DVB significantly increased DVB neurites (Extended Data Fig. 9d,e), and when tagged with GFP, localizes diffusely on the soma and neurites of DVB (Extended Data Fig. 9j). The reduction in aldicarb-induced time to spicule protraction in *nrx-1* mutants was rescued with expression of the long isoform of NRX-1 in DVB, but overexpression of NRX-1 in wildtype animals did not change time to spicule protraction compared with wildtype males (Extended Data Fig. 9f). These results indicate that the long isoform of NRX-1 is required in DVB for neurite outgrowth, and does not

require the PDZ domain, which may extend the gene's role beyond its canonical function at synapses. Varying the levels of NRX-1 in DVB directly impacts the extent of neurite outgrowth, while loss of NRX-1 in DVB reduces inhibition onto the spicule protraction circuit, such that spicule protraction occurs more rapidly.

The exuberant DVB neurite branching phenotype of *nlg-1* null mutants is completely suppressed by loss of *nrx-1* and the increases of DVB neurite branching observed upon NRX-1 overexpression is not further enhanced by loss of NLG-1. (Extended Data Fig. 9g–i). Furthermore, *nrx-1(wy778); nlg-1(ok259)* double null mutant males with NRX-1 expressed in DVB showed increased neurites, similar to *nlg-1* mutants (Extended Data Fig. 9g–i). Hence, restoring NRX-1 expression in DVB with otherwise global loss of NRX-1 and NLG-1 recapitulates NLG-1 loss alone, suggesting that the *nlg-1* phenotype requires NRX-1 in DVB. GFP-tagged NRX-1 localizes diffusely on the membrane of soma and processes and did not appear to change between days 1 and 3 (Extended Data Fig. 9j). In contrast, expression of GFP-tagged NLG-1 decreased from day 1 to 3 in muscle and neuron, the targets of DVB (Extended Data Fig. 8). Hence, NRX-1 appears to function cell-autonomously in DVB to promote DVB neurite outgrowth, while NLG-1 operates in post-synaptic partners of DVB to antagonize NRX-1-dependent growth. Decreases in NLG-1 expression may result in reduction of the antagonistic relationship, thereby permitting more NRX-1-dependent neurite elaboration. Our demonstration of an antagonistic neurexin/neuroligin relationship on neurite outgrowth may hint at a novel signaling process downstream of neurexin, which is antagonized by neuroligin and independent of neurexin's PDZ domain.

Lastly, we tested whether manipulations that induce DVB neurites in males can also induce neurites in hermaphrodite DVB. Activation of the anal depressor muscle (*gar-3b::ChR2::yfp*), loss of NLG-1, loss of NRX-1, or overexpression of NRX-1 in DVB had no impact on hermaphrodite DVB axon morphology (Extended Data Fig. 10). Cell-autonomous sexual identity changes of either DVB or postsynaptic muscles using genetic manipulations of the sex-determination pathway also did not alter DVB morphology (see Methods). Thus, sexually dimorphic morphology and plasticity of the sex-shared DVB neuron seems to be a non-autonomously instructed by male-specific circuit components.

Experience-dependent neuronal plasticity in the adult brain can include remodeling of dendrites and axons for behavioral adaptation or homeostatic maintenance of circuits. Our results for *C. elegans* male-specific DVB neurite outgrowth reveal the functional impact on circuits and behavior of morphologic remodeling. Through neurite outgrowth and rewiring of specific synapses, the DVB neuron undergoes a functional change that likely serves as an adaptive mechanism, perhaps translating experience into finer coordination of circuit activity and subsequent muscle contraction. These findings may have implications for the normal function of neurexin and neuroligin in plasticity, and for the many human diseases associated with them.

METHODS

C. elegans strains

Wild-type strains were *C. elegans* variety Bristol, strain N2. Worms were grown at 23 °C on nematode growth media (NGM) plates seeded with bacteria (*E. coli* OP50) as a food source. All males contained either *him-8(e1489) IV* or *him-5(e1490) V* as indicated by strain. Male worms were picked at the fourth larval stage onto plates with 10 other males (unless otherwise indicated), and allowed to molt into adults and age to the day indicated for each analysis or experiment.

Mutant alleles used in this study include:

him-8(e1489) IV, him-5(e1490) V, unc-31(e928) IV, nlg-1(ok259) X, nrx-1(ok1649) V, unc-119(ed3) III; nrx-1(wy778[unc-119(+)]) V, lim-6(nr2073) X, pkd-2(pt8) IV, unc-97(su110) X, unc-25(e156) III, unc-49(e407) III, nrx-1(ok1649)V, nrx-1(gk246237).

All transgenic strains used in this study are listed in Extended Data Table 1 ordered by figures and extended data figures. All plasmids were injected at 25 ng μl^{-1} with coinjection marker *ttx-3::gfp* or *ttx-3::wCherry* also at 25 ng μl^{-1} to generate extrachromosomal arrays (unless otherwise noted).

Cloning and constructs

To generate lim-6^{int4}*::wCherry* (pMG198) and *lim-6^{int4}::gfp* (pMG141), a 291 bp fragment of the *lim-6* fourth intron was amplified with primers adding BamHI to forward (CCCCGGATCCTTAGCCAGTTGCATAAATAT) and MscI to reverse (GGGGTGGCCACTAAGCTTCTTGCTAAAATTC). This fragment was digested and ligated into *pPD95.75* vector with either GFP or codon-optimized mCherry ('wCherry'). Plasmids were injected at 5 ng μl^{-1} into a *pha-1(e2123)* mutant strain with pha-1(+) coinjection marker. Extrachromosomal arrays were integrated to yield *otIs541 and otIs525. lim-6^{int4}* was found to express brightly in DVB, dimly in AVL and RIS, and dimly in about ~70% of animals in PVT.

To generate *lim-6^{int4}::gfp::rab-3 (*pMH1*), lim-6^{int4}* was PCR amplified from pMG193 using primers fwd GATGGATACGCTAACAACTTGGAAATGAAATGGATCCTTAGCCAGTTGCATAAATATTTAAAGTCAAATG and rev GAAACATACCTTTGGGTCCTTTGGCCACTAAGCTTCTTGCTAAAATTCTCTTTGATTTG, and cloned into DACR10 (a gift from D. Colon-Ramos) to replace the *ttx-3* promoter using RF cloning. The resulting plasmid was injected at 45 ng μl^{-1} with coinjection marker ttx-3::gfp also at 45 ng μl^{-1}. An extrachromosomal array was integrated to yield *otIs659.*

To generate *lim-6^{int4}::ChR2::yfp (*pMH17*), lim-6^{int4}* was PCR amplified from pMH1 using primers fwd CTAGATCAAACAAGTTTGTACAAAAAAGCTTGCATGCCTGGATCCTTAG and rev CACTTTGTACAAGAAAGCTGGGTCCTAAGCTTCTTGCTAAAATTCTCTTTG, and

cloned into pLR183 (*gar-3b::ChR2::yfp*, a gift from LR Garcia[16,30]) to replace the *gar-3b* promoter using RF cloning.

To generate *lim-6^{int4}::BirA::nrx-1^{LONG}*(pMH27*), lim-6^{int4}* was PCR amplified from pMH1 using primers fwd GAAATGAAATAAAGCTTGCATGAGCTTGCATGCCTGGATCCTTAG and rev CTTTGGGTCCTTTGGCCAATCCCGGCTAAGCTTCTTGCTAAAATTC, and cloned into pMO23[31] (*srg-13::BirA::nrx-1)* to replace the *srg-13* promoter using RF cloning.

To generate *lim-6^{int4}::BirA::nrx-1^{SHORT}*(pMH41*),* the first exon of the *nrx-1* short isoform was PCR amplified from N2 genomic DNA using primers fwd GAAGTGGAGGTGGAGGCTCCTCAGGTGTATTCCTTGAGCATTTGCGTGGTG and rev GTTGGAAGGACTGGCGAGAAGAATCCAGTAGTCTCTCCGGACACATCATTC, and cloned into pMH27 to replace the first 23 exons of the long isoform of *nrx-1* using RF cloning.

To generate *lim-6^{int4}::BirA::nrx-1^{noPDZ}*(pMH44*),* the first exon of the *nrx-1* short isoform was PCR amplified from N2 genomic DNA using primers fwd CAACGGCCACAATGATGAGAAACGGAAACGGGAATGGGGTGGCATCTCGAGGAG CTCCCGAGATCTTCAGCGCTC and rev CTACGAATGCTGAGCGCTGAAGATCTCGGGAGCTCCTCGAGATTATGCCACCCCAT TCCCGTTTC, and cloned into pMH27 to delete the last 30bp of nrx-1 cDNA before the stop codon using RF cloning.

To generate *lim-6^{int4}::GFP::nrx-1 (*pMH37*),* eGFP cDNA was PCR amplified from pMH1 using primers fwd CTATCGGAGCAGCATTCAATACTAGGCATTTGGCTCAAAAAAGACTGTTACG and rev CGACGATGACGTAACAGTCTTTTTTGAGCCAAATGCCTAGTATTGAATG, and cloned into pMH27 to replace birA cDNA using RF cloning.

To generate *lim-6^{int4}::nlg-1::gfp1-10 (*pMH18*), lim-6^{int4}* was PCR amplified from pMH1 using primers fwd CAAGCTTGCATGCGCGGCCGCACAGCTTGCATGCCTGGATCCTTAG and rev GTCCTTTGGCCAATCCCGGGGATCTAAGCTTCTTGCTAAAATTCTCTTTG, and cloned into MVC6 (*gpa-6::nlg-1::gfp1-10,* a gift from M. VanHoven) to replace the *gpa-6* promoter using RF cloning.

To generate *gar-3b::nlg-1::gfp11* (pMH20), *gar-3b promoter was* PCR amplified from pLR183 using primers fwd CAAGCTTGCATGCGCGGCCGCACCATAAGCATCATGAGCAACATCTCCACTTCTC GTGAGC and rev GTCCTTTGGCCAATCCCGGGGATGATTAATAAATGTGCAGGAGGAGTAATAATGGT GTATGT, and cloned into MVC12 (*flp-18p::nlg-1::gfp11,* a gift from M. VanHoven) to replace the *flp-18* promoter using RF cloning.

To generate *lim-6^{int4}::nlg-1::gfp11 (*pMH8*), lim-6^{int4}* was PCR amplified from pMH1 using primers fwd CAAGCTTGCATGCGCGGCCGCACAGCTTGCATGCCTGGATCCTTAG

and rev GTCCTTTGGCCAATCCCGGGGATCTAAGCTTCTTGCTAAAATTCTCTTTG, and cloned into MVC6 to replace the *gar-3b* promoter using RF cloning.

To generate *flp-13::nlg-1::gfp11 (*pMH23*),* the *flp-13* promoter was PCR amplified from N2 genomic DNA using primers fwd CAAGCTTGCATGCGCGGCCGCACGCAGTGACGTCATCTTGTTCG and rev GTCCTTTGGCCAATCCCGGGGATAAATTGTGCCTCCTGATGCTG, and cloned into pMH20 to replace the *gar-3b* promoter using RF cloning.

To generate *unc-103E::nlg-1::gfp11 (*pMH21*),* the *unc-103E* promoter was PCR amplified from N2 genomic DNA using primers fwd CAAGCTTGCATGCGCGGCCGCACTCGCGGTGCCCAAAAGGTAGGTTATTGACGTATTCTCC and rev GTCCTTTGGCCAATCCCGGGGATTACCACCACCACCACAACCACCGATCGACGAC, and cloned into pMH20 to replace the *gar-3b* promoter using RF cloning.

To generate *unc-103F::nlg-1::gfp11 (*pMH25*),* the *unc-103F* promoter was PCR amplified from N2 genomic DNA using primers fwd CAAGCTTGCATGCGCGGCCGCACCACGCCTGCCTAAGGGATGCCTTAGCTC and rev GTCCTTTGGCCAATCCCGGGGATGACATTGCCACGTGGTTGTGTGTGTG, and cloned into pMH20 to replace the *gar-3b* promoter using RF cloning.

To generate *lim-6^{int4}::HisCl1::gfp (*pMH3*),* the *lim-6^{int4}* promoter was PCR amplified from N2 genomic DNA using primers fwd GCATGCGCGGCCGCACTGACTGGGCCGGCCGGATCCTTAGCCAGTTG and rev CAATCCCGGGGATCCTCTAGAGGCGCGCCCTAAGCTTCTTGCTAAAATTC, and cloned into pNP471 to replace the *rig-3* promoter using RF cloning.

To generate *gar-3b::HisCl1::gfp (*pMH28*),* the *gar-3b* promoter was PCR amplified from pMH20 genomic DNA using primers fwd CTTGCATGCGCGGCCGCACTGACTGGGCCGGCCCATAAGCATCATGAGCAACATCTC and rev CAATCCCGGGGATCCTCTAGAGGCGCGCCAAAGCTGGGTCGATTAATAAATGTGCAG, and cloned into pMH3 to replace the *lim-6^{int4}* promoter using RF cloning.

Microscopy

Worms were anaesthetized using 100 mM of sodium azide (NaN_3) and mounted on a pad of 5% agar on glass slides. Worms were analyzed by Nomarski optics and fluorescence microscopy, using a Zeiss 880 confocal laser-scanning microscope. Multidimensional data were reconstructed as maximum intensity projections using Zeiss Zen software. Puncta were quantified by scanning the original full **Z**-stack for distinct dots in the area overlapping with the processes of the DVB neuron. Figures were prepared using Adobe Photoshop CS6 and Adobe Illustrator CS6.

Neurite tracing

Confocal **Z**-stacks were opened using FIJI, and loaded into the Simple Neurite Tracer plugin[32]. The primary neurite of DVB was traced from the center of the cell soma to the point where the axon projects ventrally and then turns anteriorly, at the final branch point before it becomes a single process. Neurites were added by tracing off of this primary neurite, including all neurites emanating posterior of the last branch point. The simple neurite tracer plugin was used to analyze the skeletons for neurite length, which were summed to calculate total neurite length, and the number of neurite junctions (a proxy for the number of neurite branches).

Cell ablation

We performed laser ablations using a MicroPoint Laser System Basic Unit (N2 pulsed laser (dye pump), ANDOR Technology) attached to a Zeiss Axioplan 2IE widefield microscope (objective EC Plan-Neofluar 100**Å**~/1.30 Oil M27). This laser delivers 120 μJoules of 337 nm energy with a 3-nsec pulse length. Ablations were performed as previously described[33], with pulse repetition rates of ~15 Hz. Cell identification was performed with GFP or Cherry markers. Ablations were performed at the days of adulthood indicated, and worms were analyzed ~20h later. Mock animals were placed on same slide under microscope but were not ablated, and were allowed to recover in a similar manner. Before relevant assays were performed (spicule protraction or aldicarb assays), worms were analyzed for loss of cell fluorescence under dissecting scope. When possible, after assays, worms were mounted on glass slides and analyzed under microscope to validate that cell-ablation was successful.

Aldicarb spicule protraction assay

Aldicarb was added to warm liquid NGM agar media for a final concentration of 5mM and poured into plates. Worms were picked 12 or fewer at a time onto aldicarb plates and observed for spicule protraction longer than 5s[13], when the time was recorded for each worm.

Mating assay

L4 male worms were picked and singled onto plates. Non-mated males were left individually on plates, while mated males had 10 *unc-31(e928)* hermaphrodites added to their plates. We exposed males to uncoordinated hermaphrodites (*unc-31*/CAPS), to ensure successful mating experience. Following 48 hours of either being housed individually or with 10 hermaphrodites, all mated plates were checked for fluorescent progeny to ensure successful mating had occurred, and then mated and non-mated (individually housed) males were subjected to confocal microscopy. *C. elegans* males housed with other males or in isolation can engage in mating-like behaviors, which may include spicule protraction. To minimize mating sensory input and self-mating behavior, we also analyzed DVB neurite outgrowth in males with mutation in *pkd-2*/PKD2[22] and in males genetically paralyzed by a mutation in *unc-97*/LIMS1 (affects body wall muscle ultrastructure)[23].

Mating behavior assay

Mating assays were based on procedures described previously[34,35]. Males were picked at the L4 stage and kept apart from hermaphrodites. One male was transferred to a plate covered with a fresh OP50 lawn containing 15 adult *unc-31(e928)* hermaphrodites. Day 1 males were less than 18 hours following L4 molt. Males were observed for 5 mins from the time of first contact with a hermaphrodite or until they ejaculated, whichever came first. Males were scored for their ability to prod the vulva, protract spicules, and transfer sperm. Mating success was calculated as 100X the number of males that transferred sperm successfully divided by the total number of males tested. Number of attempts at prodding was calculated by summing attempts at prodding for each male. Protraction/prodding ratio was calculated by dividing the number of spicule protractions by the number of attempts at prodding for each male.

Synapse visualization

GRASP plasmid construction is described above. For visualization of DVB-> spicule protraction circuit neurons and muscles, we injected *lim-6^{int4}::nlg-1::gfp1-10 (*pMH18) to label presynaptic DVB, together with *gar-3b::nlg-1::gfp11* (pMH20) to label post-synaptic SPC and spicule protractor muscles. Plasmids were injected together at 25 ng μl^{-1} with coinjection marker *ttx-3::gfp* also at 25 ng μl^{-1} to generate extrachromosomal arrays. For visualization of DVB-> flp-13p neurons/muscles, we injected *lim-6^{int4}::nlg-1::gfp1-10 (*pMH18) to label presynaptic DVB, together with *flp-13::nlg-1::gfp11 (*pMH23) to label post-synaptic spicule retractor muscles. Plasmids were injected together at 25 ng μl^{-1} with coinjection marker *ttx-3::gfp* also at 25 ng μl^{-1} to generate extrachromosomal arrays. Synapses between DVB and spicule retractor muscles were not reported in the EM of an ‘old male[36], which may be due to the observed decrease in these synapses after day 1, or these synapses may have been characterized as one of several ‘unknown’ connections of DVB from the EM[8]. The *flp-13* promoter also labels CP6 in males, which has few synapses with DVB that were located in the EM reconstruction anterior to the DVB neurites, and the branched parts of the axons of DVB and CP6 appear to not make contact (Extended Data Fig. 4h).

Spicule activation assay with channelrhodopsin

All-trans retinal was added to LB/OP50 and coated over the entire plate at a final concentration of 0.1 mM. We obtained strains expressing channelrhodopsin under the *gar-3b* promoter[17,30,37] labeling spicule protraction neurons and muscles, *unc-103E* promoter labeling spicule protractors and anal depressor muscles, and *unc-103F* promoter labeling spicule neurons SPC, PCA, and PCB[16] (gifts from LR Garcia). Worms were incubated overnight on retinal plates before all assays involving channelrhodopsin containing strains. For spicule protraction assay, male worms on retinal plates were individually subjected to 488 nm light for 10 seconds 3 times with 30 seconds between trials on a Nikon eclipse E400 microscope. Obvious spicule muscle contraction for any of the 3 trials was recorded as a response. Videos were recorded using a mounted Exo Labs Focus camera. For activation protocol, male worms on retinal plates were subjected to alternating 488 nm light 3 times (15s light/15s dark) on a Leica M165 FC dissecting scope, and repeated every 45 minutes

for 4.5 hours. Worms were then subjected to confocal microscopy or aldicarb behavioral assay. Controls for neurite outgrowth and aldicarb behavior were performed on males under the same conditions but not exposed to the channelrhodopsin cofactor all-*trans* retinal (Extended Data Fig. 5j–l). Worms for recovery were placed in dark for ~20 hours following activation protocol, then subjected to the same analysis. A small number of individual males subjected to confocal imaging before and after activation, or after activation and following recovery demonstrated addition of neurites following activation, and removal of neurites following recovery, however the difficulty of this analysis precluded quantification.

Neuronal silencing with histamine chloride channel (HisCl1)

Control or transgenic animals were picked onto normal NGM media plates seeded with OP50 at L4 stage, then picked the evening before the indicated day of analysis onto 10 mM histamine or control plates with OP50 bacteria as food source. For *gar-3b::HisCl1* silencing assays, males were left on histamine or control plates overnight then subjected to confocal microscopy the following morning. For *lim-6^{int4}::HisCl1* defecation analysis, males were picked onto histamine plates, allowed to adjust for 5 minutes then analyzed for defecation behavior. Histamine plates were prepared as previously described[12].

Defecation assay

Males were placed on control or 10mM histamine plates with food on day of analysis, allowed to explore for 5 minutes, then observed for 10–12 minutes on a low magnification Leica MZ8 light dissecting microscope. Expulsion steps were recorded for time between consecutive expulsions, and the presence of spicule protraction within +/− 3 seconds of expulsion. The percentage of expulsion steps associated with spicule protraction was calculated for each male. The time between consecutive expulsion steps was calculated by averaging all times recorded between consecutive expulsions for each male.

Exogenous GABA exposure

Males were picked onto normal NGM media plates seeded with OP50 at L4 stage, then picked before day of analysis onto 30mM GABA[10] or control plates seeded with OP50, and left overnight, then subjected to confocal microscopy. For 3 day GABA exposure, males were picked onto 30mM GABA or control plates seeded with OP50, left for 3 days and then subjected to confocal microscopy.

Measurement of fluorescence intensity

For quantification of fluorescence intensity of *nlg-1p::nlg-1::gfp*, a stack of images was acquired using confocal microscopy using the same acquisition parameters between samples (objective, pixel size, laser intensity, pinhole size, PMT settings). The fluorescence intensity mean was obtained using ZEN Black software. For the dorsal spicule muscles, the muscles were outlined and the cross-section with the highest mean was recorded. Dorsal spicule muscles include the gubernacular retractor, gubernacular erector, anterior oblique, anal depressor, which could be outlined easily, whereas the spicule protractor could not always be observed in males after day 1. For the pre-anal ganglion and the DVB/background, a pre-defined circle was used to outline the region of interest, and the cross section with the

highest mean was recorded. The ratio of fluorescence intensity was calculated by dividing the mean of the dorsal spicule muscles (arbitrary units) by the mean of the DVB/background (arbitrary units) or by dividing the mean of the pre-anal ganglion by the mean of the DVB/background (arbitrary units).

Cell-autonomous changes in sexual identity

We tested cell-autonomous changes in sexual identity of DVB (*lim-6*^{int4} promoter) and muscles (*myo-3* promoter) by expressing the cDNA of either *fem-3* in hermaphrodites to masculinize each tissue, or the cDNA of *tra-2* $^{\text{intracellular domain}}$ in males to feminize each tissue[38–40]. In males with feminized DVB or muscles we observed no suppression of DVB neurites, and in hermaphrodites with masculinized DVB or muscle we observed no induction of DVB neurites.

Statistics and reproducibility

We performed two-tailed Student's ttest or one-way ANOVA with post-hoc Tukey HSD test using *R* and *RStudio*, p-values shown on each graph. No statistical methods were used to predetermine sample size, and the experiments were not randomized. Number of independent replicates = Figure 1 b/c/d- 7. Figure 2 a/b/c/h/i/j/k- 3 or more, e/f- 2 or more. Figure 3 a/b/c/d/e/f/g- 3 or more. Figure 4 a/b/c/d/e/f/g/h- 3 or more. Ex Data Figure 1 a/b/c- 4 or more, d- 2 or more. Ex Data Figure 2 a/b- 4 or more, c/d/e/f/g/h - 2 or more. Ex Data Figure 3 a/b/c- 3 or more, d-f- 2 or more. Ex Data Figure 4 a/b/c/h- 2 or more, d/e/f/g – 3 or more. Ex Data Figure 5 a/b/c/d/e/f- 4 or more, g/h/i/j/k/l - 2 or more. Ex Data Figure 6 a/b/c/d/e/f- 2 or more. Ex Data Figure 7 a/b/c/d/e/f/g/h- 3 or more. Ex Data Figure 8 a/b/c-3 or more, d/e/f – 2 or more. Ex Data Figure 9 b/c/d/r/f/gh/i- 3 or more, j-2 or more. Ex Data Figure 10 a/b/c- 3 or more.

Data Availability Statement

The data that support the findings of this study are available from the corresponding author upon reasonable request.

Extended Data

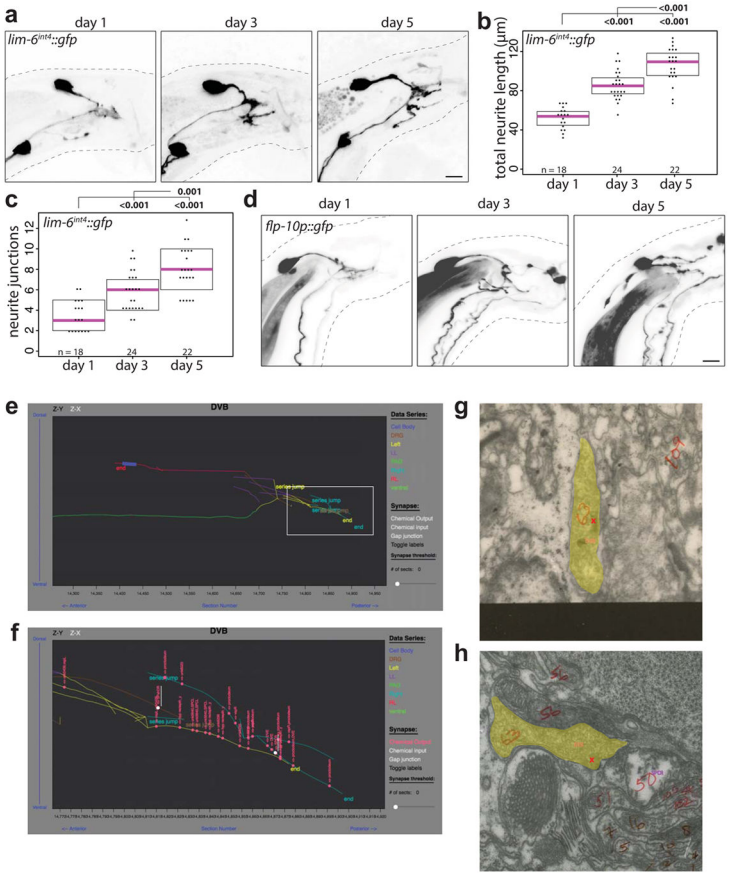

Extended Data Fig. 1. Progressive neurite outgrowth in DVB in adulthood

(a) DVB neuron visualized with *lim-6*^{int4}*::gfp* at days 1, 3, and 5 in adult males and quantified by **(b)** total neurite length and **(c)** number of neurite junctions (dot=one animal, magenta bar=median, and boxes=quartiles, one-way ANOVA and post-hoc Tukey HSD). **(d)** DVB neurite outgrowth visualized with *flp-10::gfp* in males at days 1, 3, and 5 of adulthood (n>10). **(e)** Tracing reconstruction of male DVB from EM sections compiled by wormwiring.org showing DVB neurites. **(f)** Inset of DVB neurites showing pre-synaptic specializations identified in EM sections shown in pink. EM section showing DVB pseudo-colored yellow with pre-synaptic specialization indicated with red ‘x’ with **(g)** SPCR (Image Right1200, Section 14871) and **(h)** spicule sheath (Image N2YDRG1175, Section 14816), shown in white in inset panel.

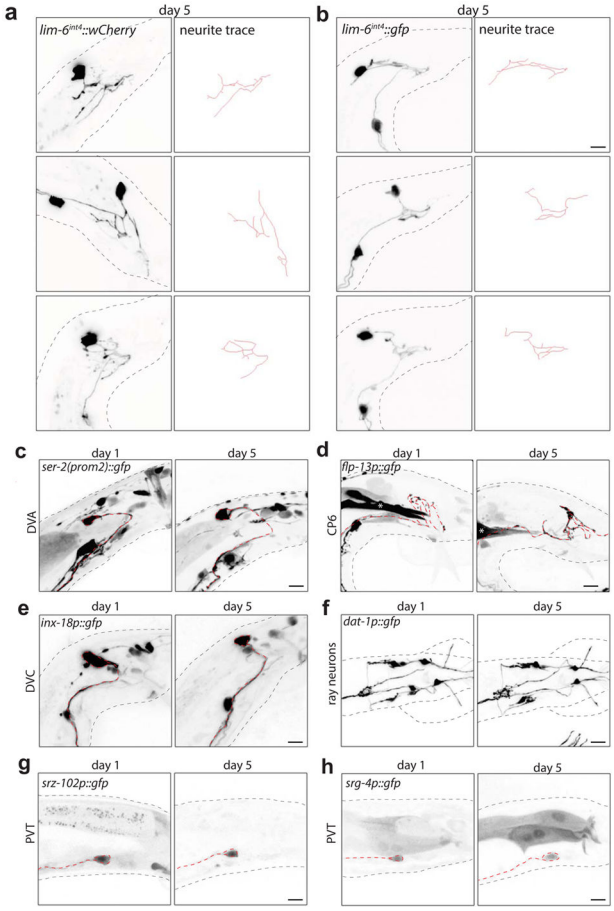

Extended Data Fig. 2. DVB neurite outgrowth in adult male *C. elegans* is stochastic and other neurons in the male tail do not show progressive neurite outgrowth in adulthood

DVB neurites at day 5 visualized with **(a)** *lim-6^{int4}::wCherry* or **(b)** *lim-6^{int4}::gfp* (n>10 for each). DVB posterior neurites were traced through confocal stacks using Simple Neurite Tracer[4] plugin. **(c)** DVA neuron visualized with *ser-2(prom-2)::gfp* (n=5)(red dashed line indicates axon of relevant neuron), **(d)** DVC neuron visualized with *inx-18p::gfp* (n=5), **(e)** CP6 neuron visualized with *flp-13::gfp* (cell soma not shown) (n=5), **(f)** ray neurons visualized with *dat-1::gfp* (ventral view)(n=5). PVT neuron visualized with *srz-102p::gfp* (n=5)**(g)** and *srg-4p::gfp* (n=5)**(h)** at day 1 and day 5. Axons of indicated neurons highlighted by red dashed line.

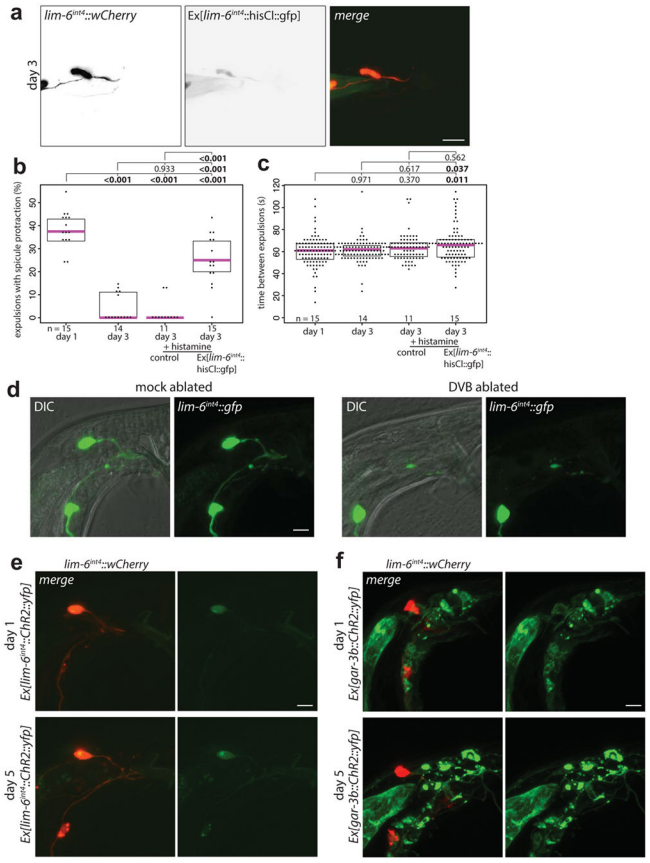

Extended Data Fig. 3. DVB inhibits expulsion-associated spicule protraction at day 3. Laser ablation of DVB and Channelrhodopsin expression in DVB and spicule protraction circuit

(a) Confocal images of male worm with *lim-6^{int4}::wCherry* and *lim-6^{int4}::HisCl1::gfp* at day 3 and **(b)** quantification of the percentage of expulsion steps with spicule protraction for day 1 control, day 3 control, day 3 control + histamine, and day 3 *lim-6^{int4}::HisCl1::gfp* + histamine males. **(c)** Quantification of time between consecutive expulsion steps for day 1 control, day 3 control, day 3 control + histamine, and day 3 *lim-6^{int4}::HisCl1::gfp* + histamine males (+ histamine = 10mM histamine plates)(dot=one animal, magenta bar=median, and boxes=quartiles, one-way ANOVA and post-hoc Tukey HSD). **(d)** Confocal images of male worms with or without laser ablation of DVB at day 1–2, visualized with *lim-6^{int4}::gfp*. **(e)** Confocal images of DVB (*lim-6^{int4}::wCherry)* expressing channelrhodopsin at day 1 and 5, Ex[*lim-6^{int4}::ChR2::yfp].* **(f)** Confocal images of DVB (*lim-6^{int4}::wCherry)* and spicule circuit expressing channelrhodopsin at day 1 and 5, Ex[*gar-3b::ChR2::yfp].* (n>10 for d, e, and f).

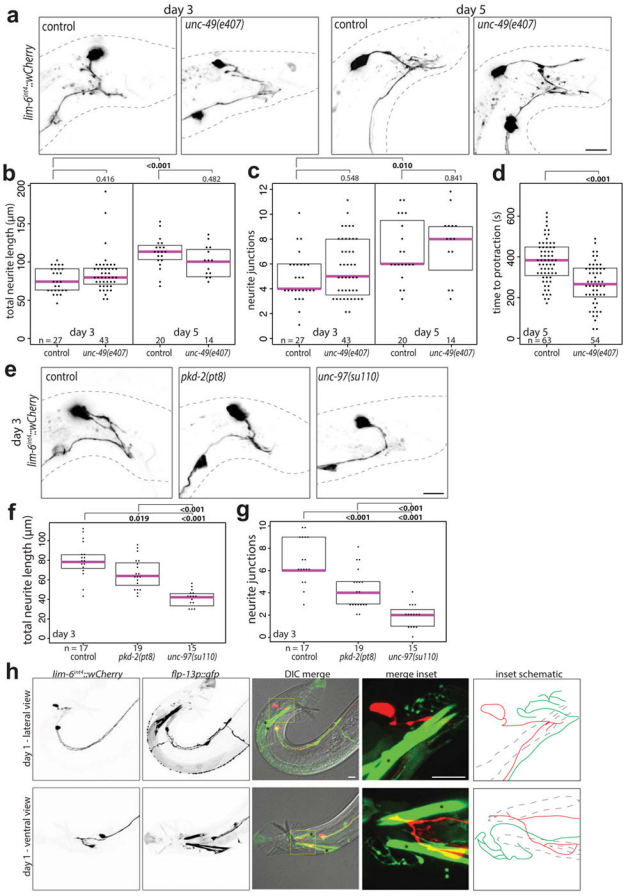

Extended Data Fig. 4. DVB neurite outgrowth in *unc-49*, *pkd-2* and *unc-97* mutant males. *flp-13p::gfp* labels CP6 and spicule retractor muscles

(a) Confocal images and quantification of **(b)** total neurite outgrowth and **(c)** number of neurite junctions in control and *unc-49(e407)* males at days 3 and 5. **(d)** Time to spicule protraction on aldicarb at day 5 for control and *unc-49(e407)* males. **(e)** Confocal images and quantification of **(f)** total neurite outgrowth and **(g)** number of neurite junctions in control, *pkd-2(pt8), and unc-97(su110)* males at day 3. **(h)** Confocal images of male worms with *lim-6*^{int4}*::wCherry, flp-10p::gfp,* and DIC at day 1 in ventral and lateral views. Inset showing DVB and CP6 axons, with schematic of axons demonstrating lack of contact (red is DVB axon, green is CP6 axon, blue dashed lines are spicule retractor muscles). Asterisks in *flp-13::gfp* panel mark spicule retractor muscles. (dot=one animal, magenta bar=median, and boxes=quartiles, one-way ANOVA and post-hoc Tukey HSD).

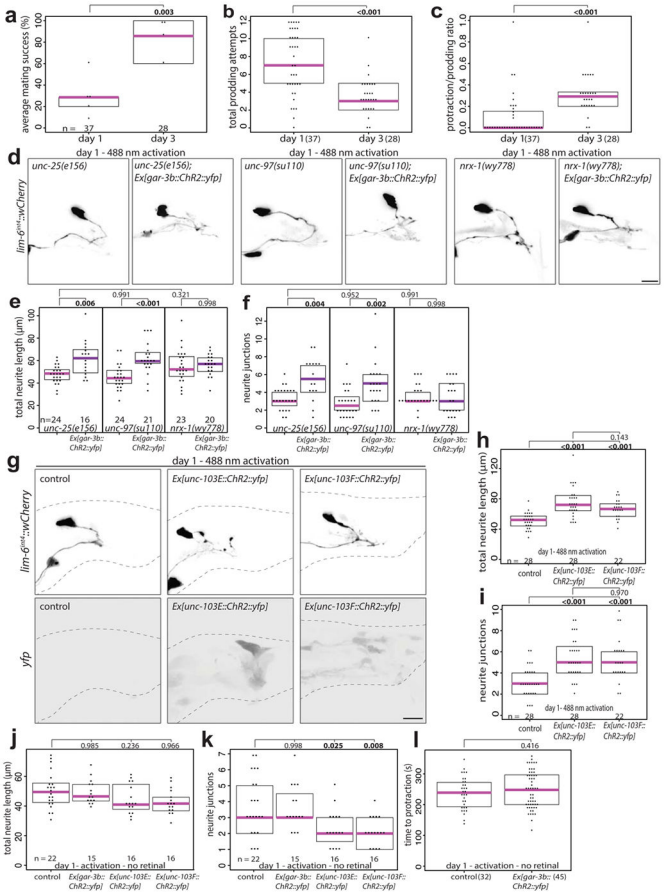

Extended Data Fig. 5. Day 1 male mating defects involving spicule coordination, spicule circuit activation in *unc-25*, *unc-97*, and *nrx-1* mutant males, and spicule neuron or muscle activation induces DVB neurite outgrowth

(a) Quantification of percentage of average mating success (sperm transfer) for day 1 and 3 males during 5-minute timed mating assays with 15 *unc-31(e928)* hermaphrodites (number of worms indicated with n=, data points represent average percentage for each replicate of multiple males). **(b)** Quantification of attempts at spicule prodding during 5-minute timed mating assay for day 1 and 3 males. **(c)** Ratio of protraction/prodding attempts during 5-minute timed mating assay for males at day 1 and 3. **(d)** Confocal images of *lim-6^{int4}::wCherry*, **(e)** total neurite length, and **(f)** number or neurite junctions of *unc-25(e156), unc-25(e156); Ex[gar-3b::ChR2::yfp], unc-97(su110), unc-97(su110); Ex[gar-3b::ChR2::yfp], nrx-1(wy778), and nrx-1(wy778); Ex[gar-3b::ChR2::yfp]* males following activation at day 1 (488 nm light for 3×15s every 45 mins for 4.5h). **(g)** Confocal images and quantification of **(h)** total neurite outgrowth and **(i)** number of neurite junctions in control, Ex[*unc-103E::ChR2::yfp], and* Ex[*unc-103F^{4}::ChR2::yfp]* after activation at day 1 with retinal (488 nm light for 3×15s every 45 mins for 4.5h). Quantification of **(j)** total neurite outgrowth and **(k)** number of neurite junctions at day 1 in control, Ex[*lim-6^{int4}::ChR2::yfp]*(DVB), Ex[*unc-103E::ChR2::yfp]*(neuron-specific), *and* Ex[*unc-103F^{4}::ChR2::yfp]*(muscle-specific) males after activation but in absence of retinal. **(l)** Time to protraction of control and Ex[*lim-6^{int4}::ChR2::yfp]* males after day 1 activation

in absence of retinal. (dot=one animal, magenta bar=median, and boxes=quartiles, one-way ANOVA and post-hoc Tukey HSD).

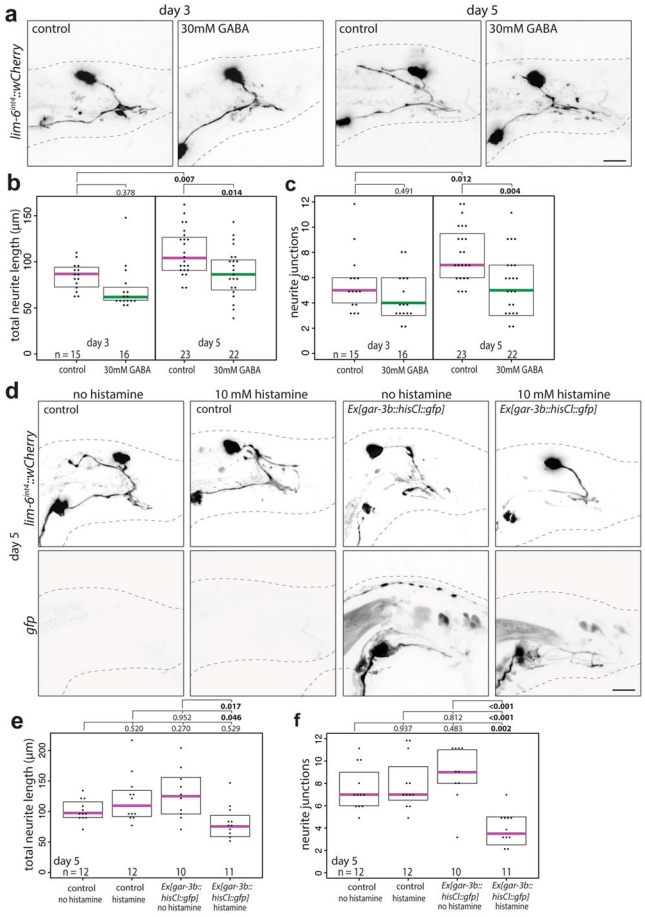

Extended Data Fig. 6. Exposure to exogenous GABA or silencing spicule protraction circuit activity overnight reduces DVB neurites on day 5

(a) Confocal images of *lim-6^{int4}::wCherry*, **(b)** total neurite length, and **(c)** number or neurite junctions of males exposed overnight to 30mM GABA at days 3 and 5. **(d)** Confocal images of *lim-6^{int4}::wCherry*, **(e)** total neurite length, and **(f)** number or neurite junctions at day 5 of control +/− overnight 10mM histamine, and *gar-3b::HisCl1::gfp* +/− overnight 10mM histamine. (dot=one animal, magenta bar=median, and boxes=quartiles, one-way ANOVA and post-hoc Tukey HSD).

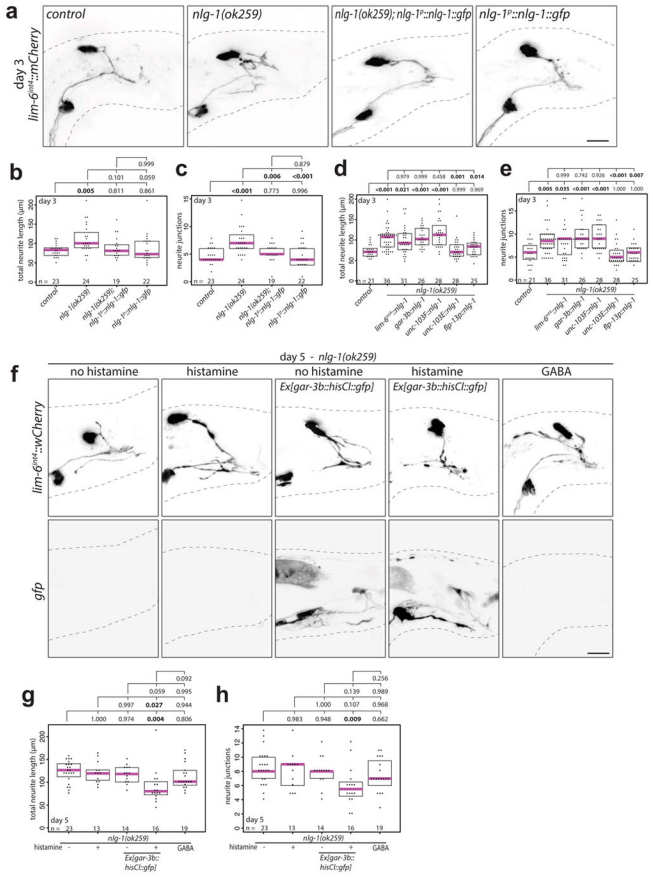

Extended Data Fig. 7. NLG-1 expression in multiple male sex muscles rescues *nlg-1* mutant DVB neurite phenotype. Silencing spicule circuit or exposure to exogenous GABA does not reduce DVB neurites in *nlg-1* mutant males

(a) Confocal images of DVB (*lim-6^{int4}::wCherry)*, and quantification of **(b)** total neurite outgrowth and **(c)** number of neurite junctions in control, *nlg-1*(ok259)*, and nlg-1(*ok259*); nlg-1p::nlg-1::gfp,* and *nlg-1p::nlg-1::gfp* day 3 males. Quantification of **(d)** total neurite outgrowth and **(e)** number of neurite junctions in control or *nlg-1*(ok259) mutant males with or without NLG-1 tissue-specific expression. Expression patterns for rescue promoters - *lim-6^{int4}* – DVB, *gar-3b* – SPC, spicule protractor muscles; *unc-103F* – SPC, PCA, PCB, other neurons; *unc-103E* – male sex muscles; *flp-13* – spicule retractor muscles, CP6. **(f)** Confocal images of *lim-6^{int4}::wCherry* and Ex[*gar-3b::HisCl1::gfp*], **(g)** total neurite length, and **(h)** number of neurite junctions of *nlg-1(ok259)* +/− 10mM histamine overnight, *nlg-1(ok259); gar-3b::HisCl1::gfp* +/− 10mM histamine overnight, and *nlg-1(ok259)* + 30mM GABA overnight in day 5 males. (dot=one animal, magenta bar=median, and boxes=quartiles, one-way ANOVA and post-hoc Tukey HSD).

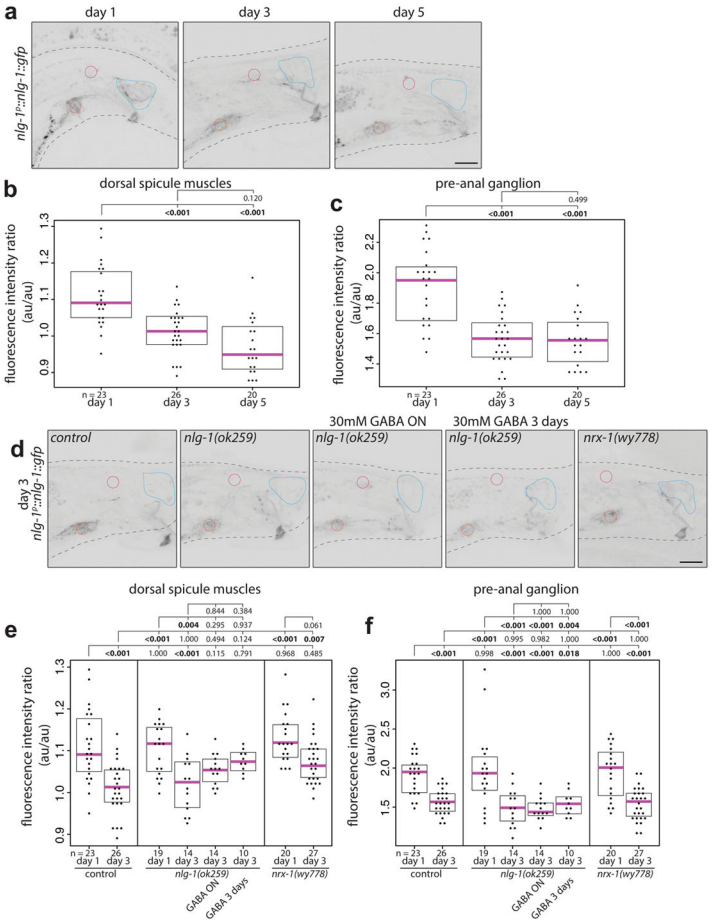

Extended Data Fig. 8. NLG-1 expression decreases from day 1 to day 3

(a) Confocal images of *nlg-1p::nlg-1::gfp* in males at day 1, 3, and 5. Example regions of interest for measurements taken from single planes – blue – dorsal spicule muscles, red – pre-anal ganglion, magenta – DVB. Quantification of fluorescence intensity of *nlg-1p::nlg-1::gfp* in males at day 1, 3, and 5 reported as a ratio of mean fluorescence in **(b)** dorsal spicule muscles or **(c)** pre-anal ganglion normalized to background of DVB, which has little to undetectable expression. Dorsal spicule muscles refer to the gubernacular retractor, gubernacular erector, anterior oblique, anal depressor. **(d)** Confocal images of *nlg-1p::nlg-1::gfp* in control, *nlg-1(ok259)*, *nlg-1(ok259)* with overnight GABA exposure, *nlg-1(ok259)* with 3 day GABA exposure, and *nrx-1(wy778)* males at day 3. Quantification of fluorescence intensity of *nlg-1p::nlg-1::gfp* in day 1 and 3 control, *nlg-1(ok259)*, and *nrx-1(wy778)* males and day 3 *nlg-1(ok259)* with overnight GABA exposure and *nlg-1(ok259)* with 3 day GABA exposure, as a ratio of mean fluorescence in **(e)** dorsal spicule muscles or **(f)** pre-anal ganglion normalized to background of DVB. (dot=one animal, magenta bar=median, and boxes=quartiles, one-way ANOVA and post-hoc Tukey HSD).

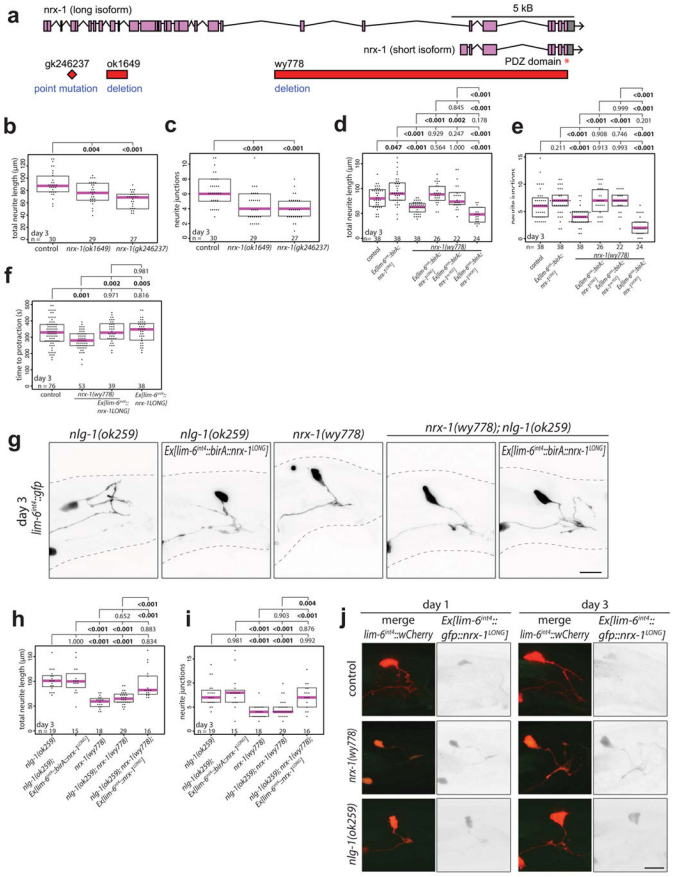

Extended Data Fig. 9. NRX-1 long isoform functions in DVB to control DVB neurite outgrowth and NRX-1 expression in DVB controls neurite outgrowth of *nlg-1* mutants

(a) Genetic loci of *nrx-1* showing long and short isoforms, PDZ domain, and location of point mutation *gk246237,* and deletions *ok1649* and *wy778*. Quantification of **(b)** total neurite length and **(c)** number of neurite junctions in controls and long-isoform specific mutants *nrx-1(ok1649)* and *nrx-1(gk246237)* at day 3. Quantification of **(d)** total neurite outgrowth and **(e)** number of neurite junctions at day 3 in control, Ex[*lim-6*^{int4}*::birA::nrx-1*^{LONG}], *nrx-1(wy778), nrx-1(wy778);* Ex[*lim-6*^{int4}*::birA::nrx-1*^{LONG}], *nrx-1*(wy778); Ex[*lim-6*^{int4}*::birA::nrx-1*^{SHORT}], *nrx-1*(wy778); Ex[*lim-6*^{int4}*::birA::nrx-1*^{noPDZ}]. **(f)** Time to spicule protraction at day 3 in control, *nrx-1*(wy778), *nrx-1*(wy778); Ex[*lim-6*^{int4}*::birA::nrx-1*^{LONG}], and Ex[*lim-6*^{int4}*::birA::nrx-1*^{LONG}]. **(g)** Confocal images of *lim-6*^{int4}*::wCherry* expression, and quantification of **(h)** total neurite length and **(i)** number of neurite junctions of day 3 *nlg-1(ok259), nlg-1(ok259);* Ex[*lim-6*^{int4}*::birA::nrx-1*^{LONG}], *nrx-1(wy778), nrx-1(wy778); nlg-1(ok259), nrx-1(wy778); nlg-1(ok259);* Ex[*lim-6*^{int4}*::birA::nrx-1*^{LONG}] males. **(j)** Confocal images of *lim-6*^{int4}*::wCherry* and Ex[*lim-6*^{int4}*::gfp::nrx-1*^{LONG}] in control, *nrx-1(wy778),* and *nlg-1(ok259)* males at day 1 and 3. (dot=one animal, magenta bar=median, and boxes=quartiles, one-way ANOVA and post-hoc Tukey HSD).

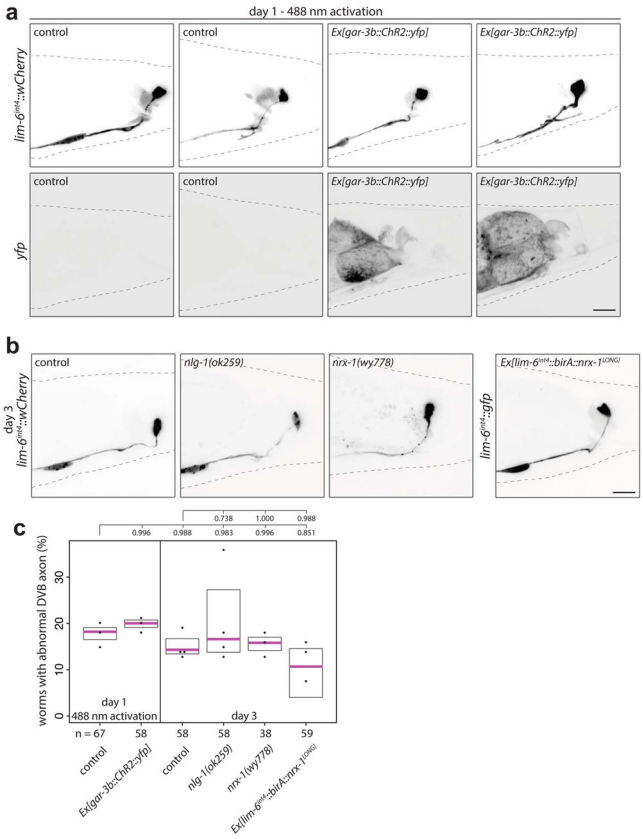

Extended Data Fig. 10. DVB in hermaphrodites does not show neurite branching upon *gar-3b::ChR2::yfp* activation or NRX-1/NLG-1 manipulations

(a) Confocal images of *lim-6^{int4}::wCherry* and Ex[*gar-3b::ChR2::yfp*] expression in day 1 hermaphrodites showing DVB axon projection after activation on retinal (488 nm light for 3×15s every 45 mins for 4.5h). **(b)** Confocal images of *lim-6^{int4}::wCherry* or *lim-6^{int4}::gfp* in control, *nrx-1(wy778), nlg-1(ok259),* and Ex[*lim-6^{int4}::gfp::nrx-1^{LONG}*] hermaphrodites at day 3. **(c)** Quantification of the percentage of hermaphrodites with DVB axon abnormalities, neurites (in almost all cases, a single neurite off axon just posterior of the pre-anal ganglion) in day 1 control and Ex[*gar-3b::ChR2::yfp*] with activation, day 3 control, *nrx-1(wy778), nlg-1(ok259),* and Ex[*lim-6^{int4}::gfp::nrx-1^{LONG}*]. (number of worms indicated with n=, data points represent average percentage for each replicate of multiple hermaphrodites). (dot=one animal, magenta bar=median, and boxes=quartiles, one-way ANOVA and post-hoc Tukey HSD).

Supplementary Material

Refer to Web version on PubMed Central for supplementary material.

Acknowledgments

We thank Q. Chen for generating transgenic strains and M. Gendrel for DVB promoter and reporter lines; P. Sengupta, T.G. Drivas, M. Oren-Suissa, and members of the Hobert lab for comments on the manuscript. L.R. Garcia and K. Shen for worm strains and M. VanHoven and D. Colon-Ramos for plasmids. This work supported by NIH grants from NINDS (MH:F32NS086285; OH:2R37NS039996). Oliver Hobert is a Howard Hughes Medical

Institute investigator. Some strains were provided by the CGC, funded by NIH Office of Research Infrastructure Programs (P40 OD010440).

References

1. Fu M, Zuo Y. Experience-dependent structural plasticity in the cortex. Trends Neurosci. 2011; 34:177–187. DOI: 10.1016/j.tins.2011.02.001 [PubMed: 21397343]
2. Holtmaat A, Svoboda K. Experience-dependent structural synaptic plasticity in the mammalian brain. Nat Rev Neurosci. 2009; 10:647–658. DOI: 10.1038/nrn2699 [PubMed: 19693029]
3. Vitureira N, Goda Y. Cell biology in neuroscience: the interplay between Hebbian and homeostatic synaptic plasticity. J Cell Biol. 2013; 203:175–186. DOI: 10.1083/jcb.201306030 [PubMed: 24165934]
4. Yin J, Yuan Q. Structural homeostasis in the nervous system: a balancing act for wiring plasticity and stability. Front Cell Neurosci. 2014; 8:439. [PubMed: 25653587]
5. Lee WC, et al. Dynamic remodeling of dendritic arbors in GABAergic interneurons of adult visual cortex. PLoS Biol. 2006; 4:e29. [PubMed: 16366735]
6. Marik SA, Yamahachi H, Meyer zum Alten Borgloh S, Gilbert CD. Large-scale axonal reorganization of inhibitory neurons following retinal lesions. J Neurosci. 2014; 34:1625–1632. DOI: 10.1523/JNEUROSCI.4345-13.2014 [PubMed: 24478346]
7. Keck T, et al. Loss of sensory input causes rapid structural changes of inhibitory neurons in adult mouse visual cortex. Neuron. 2011; 71:869–882. DOI: 10.1016/j.neuron.2011.06.034 [PubMed: 21903080]
8. Jarrell TA, et al. The connectome of a decision-making neural network. Science. 2012; 337:437–444. DOI: 10.1126/science.1221762 [PubMed: 22837521]
9. White JG, Southgate E, Thomson JN, Brenner S. The structure of the nervous system of the nematode Caenorhabditis elegans. Philos Trans R Soc Lond B Biol Sci. 1986; 314:1–340. [PubMed: 22462104]
10. Reiner DJ, Thomas JH. Reversal of a muscle response to GABA during C. elegans male development. J Neurosci. 1995; 15:6094–6102. [PubMed: 7666193]
11. LeBoeuf B, Garcia LR. Caenorhabditis elegans Male Copulation Circuitry Incorporates Sex-Shared Defecation Components To Promote Intromission and Sperm Transfer. G3 (Bethesda). 2017; 7:647–662. DOI: 10.1534/g3.116.036756 [PubMed: 28031243]
12. Pokala N, Liu Q, Gordus A, Bargmann CI. Inducible and titratable silencing of Caenorhabditis elegans neurons in vivo with histamine-gated chloride channels. Proc Natl Acad Sci U S A. 2014; 111:2770–2775. DOI: 10.1073/pnas.1400615111 [PubMed: 24550306]
13. Garcia LR, Mehta P, Sternberg PW. Regulation of distinct muscle behaviors controls the C. elegans male's copulatory spicules during mating. Cell. 2001; 107:777–788. [PubMed: 11747813]
14. Hobert O, Tessmar K, Ruvkun G. The Caenorhabditis elegans lim-6 LIM homeobox gene regulates neurite outgrowth and function of particular GABAergic neurons. Development. 1999; 126:1547–1562. [PubMed: 10068647]
15. Feinberg EH, et al. GFP Reconstitution Across Synaptic Partners (GRASP) defines cell contacts and synapses in living nervous systems. Neuron. 2008; 57:353–363. DOI: 10.1016/j.neuron.2007.11.030 [PubMed: 18255029]
16. Liu Y, et al. A cholinergic-regulated circuit coordinates the maintenance and bi-stable states of a sensory-motor behavior during Caenorhabditis elegans male copulation. PLoS Genet. 2011; 7:e1001326. [PubMed: 21423722]
17. Liu Y, LeBoeuf B, Garcia LR. G alpha(q)-coupled muscarinic acetylcholine receptors enhance nicotinic acetylcholine receptor signaling in Caenorhabditis elegans mating behavior. J Neurosci. 2007; 27:1411–1421. DOI: 10.1523/JNEUROSCI.4320-06.2007 [PubMed: 17287516]
18. Jobson MA, et al. Spillover transmission is mediated by the excitatory GABA receptor LGC-35 in C. elegans. J Neurosci. 2015; 35:2803–2816. DOI: 10.1523/JNEUROSCI.4557-14.2015 [PubMed: 25673867]

19. Garcia LR, Sternberg PW. Caenorhabditis elegans UNC-103 ERG-like potassium channel regulates contractile behaviors of sex muscles in males before and during mating. J Neurosci. 2003; 23:2696–2705. [PubMed: 12684455]
20. Guo X, Navetta A, Gualberto DG, Garcia LR. Behavioral decay in aging male C. elegans correlates with increased cell excitability. Neurobiol Aging. 2012; 33:1483 e1485–1423. DOI: 10.1016/j.neurobiolaging.2011.12.016
21. LeBoeuf B, Garcia LR. Cell excitability necessary for male mating behavior in Caenorhabditis elegans is coordinated by interactions between big current and ether-a-go-go family K(+) channels. Genetics. 2012; 190:1025–1041. DOI: 10.1534/genetics.111.137455 [PubMed: 22174070]
22. Barr MM, et al. The Caenorhabditis elegans autosomal dominant polycystic kidney disease gene homologs lov-1 and pkd-2 act in the same pathway. Curr Biol. 2001; 11:1341–1346. [PubMed: 11553327]
23. Hobert O, Moerman DG, Clark KA, Beckerle MC, Ruvkun G. A conserved LIM protein that affects muscular adherens junction integrity and mechanosensory function in Caenorhabditis elegans. J Cell Biol. 1999; 144:45–57. [PubMed: 9885243]
24. Bang ML, Owczarek S. A matter of balance: role of neurexin and neuroligin at the synapse. Neurochem Res. 2013; 38:1174–1189. DOI: 10.1007/s11064-013-1029-9 [PubMed: 23559421]
25. Mackowiak M, Mordalska P, Wedzony K. Neuroligins, synapse balance and neuropsychiatric disorders. Pharmacol Rep. 2014; 66:830–835. DOI: 10.1016/j.pharep.2014.04.011 [PubMed: 25149987]
26. Pizzarelli R, Cherubini E. Alterations of GABAergic signaling in autism spectrum disorders. Neural Plast. 2011; 2011:297153. [PubMed: 21766041]
27. Chih B, Engelman H, Scheiffele P. Control of excitatory and inhibitory synapse formation by neuroligins. Science. 2005; 307:1324–1328. DOI: 10.1126/science.1107470 [PubMed: 15681343]
28. Maro GS, et al. MADD-4/Punctin and Neurexin Organize C. elegans GABAergic Postsynapses through Neuroligin. Neuron. 2015; 86:1420–1432. DOI: 10.1016/j.neuron.2015.05.015 [PubMed: 26028574]
29. Haklai-Topper L, et al. The neurexin superfamily of Caenorhabditis elegans. Gene Expr Patterns. 2011; 11:144–150. DOI: 10.1016/j.gep.2010.10.008 [PubMed: 21055481]
30. LeBoeuf B, Correa P, Jee C, Garcia LR. Caenorhabditis elegans male sensory-motor neurons and dopaminergic support cells couple ejaculation and post-ejaculatory behaviors. Elife. 2014; 3
31. Oren-Suissa M, Bayer EA, Hobert O. Sex-specific pruning of neuronal synapses in Caenorhabditis elegans. Nature. 2016; 533:206–211. DOI: 10.1038/nature17977 [PubMed: 27144354]
32. Longair MH, Baker DA, Armstrong JD. Simple Neurite Tracer: open source software for reconstruction, visualization and analysis of neuronal processes. Bioinformatics. 2011; 27:2453–2454. DOI: 10.1093/bioinformatics/btr390 [PubMed: 21727141]
33. Fang-Yen C, Gabel CV, Samuel AD, Bargmann CI, Avery L. Laser microsurgery in Caenorhabditis elegans. Methods Cell Biol. 2012; 107:177–206. DOI: 10.1016/B978-0-12-394620-1.00006-0 [PubMed: 22226524]
34. Garcia LR, LeBoeuf B, Koo P. Diversity in mating behavior of hermaphroditic and male-female Caenorhabditis nematodes. Genetics. 2007; 175:1761–1771. DOI: 10.1534/genetics.106.068304 [PubMed: 17277358]
35. Hilliard MA, Bargmann CI, Bazzicalupo PC. elegans responds to chemical repellents by integrating sensory inputs from the head and the tail. Curr Biol. 2002; 12:730–734. [PubMed: 12007416]
36. Sulston JE, Albertson DG, Thomson JN. The Caenorhabditis elegans male: postembryonic development of nongonadal structures. Dev Biol. 1980; 78:542–576. [PubMed: 7409314]
37. Correa P, LeBoeuf B, Garcia LRC. elegans dopaminergic D2-like receptors delimit recurrent cholinergic-mediated motor programs during a goal-oriented behavior. PLoS Genet. 2012; 8:e1003015. [PubMed: 23166505]
38. White JQ, et al. The sensory circuitry for sexual attraction in C. elegans males. Curr Biol. 2007; 17:1847–1857. DOI: 10.1016/j.cub.2007.09.011 [PubMed: 17964166]
39. Lee K, Portman DS. Neural sex modifies the function of a C. elegans sensory circuit. Curr Biol. 2007; 17:1858–1863. DOI: 10.1016/j.cub.2007.10.015 [PubMed: 17964163]

40. Mowrey WR, Bennett JR, Portman DS. Distributed effects of biological sex define sex-typical motor behavior in Caenorhabditis elegans. J Neurosci. 2014; 34:1579–1591. DOI: 10.1523/JNEUROSCI.4352-13.2014 [PubMed: 24478342]

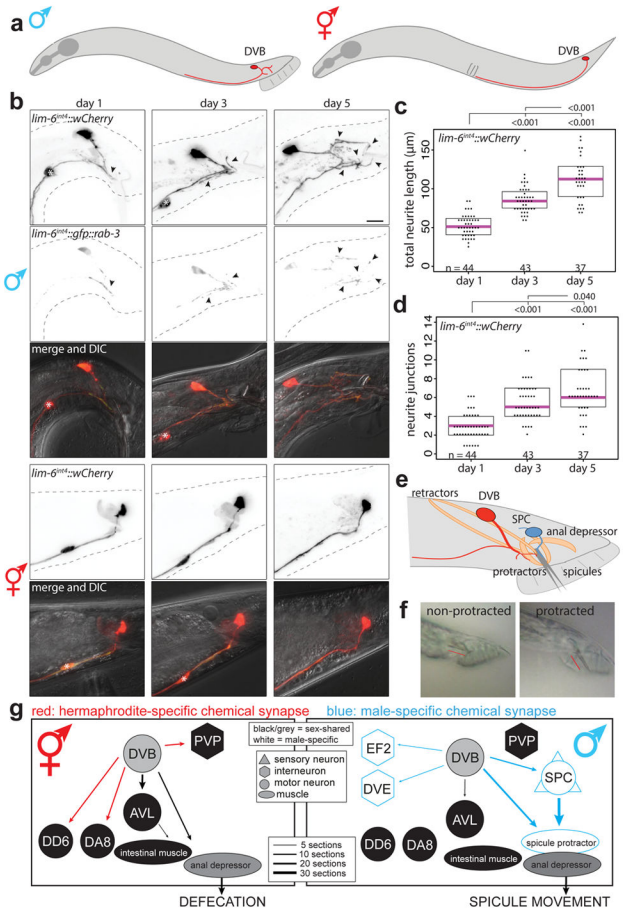

Fig. 1. Progressive neurite outgrowth of the GABAergic DVB neuron in adult males

(a) DVB neuron schematic. **(b)** DVB visualized with *lim-6*^{int4}*::wCherry* during adulthood in males and hermaphrodites (asterisk=PVT neuron, arrowheads=DVB neurites, scale bar=10 µm(true for all subsequence figures), n same as **(c)**). Presynaptic boutons visualized with presynaptic marker *lim-6*^{int4}*::gfp::rab-3*. DVB neurite outgrowth quantified by **(c)** total neurite length and **(d)** number of neurite junctions (dot=one animal, magenta bar=median, and boxes=quartiles. Comparison using one-way ANOVA and post-hoc Tukey HSD, p-values and n shown). **(e)** Schematic of DVB and post-synaptic spicule-associated neurons and muscles in male tail. **(f)** Example demonstrating males with normal or protracted spicules (red line indicates spicule(n>10)). **(g)** Connectivity of DVB at adult stage inferred from electron micrographs[8,11]. Chemical synapses depicted as arrows, black arrows and neurons are sex-shared, red are hermaphrodite-specific, blue are male-specific. Behavioral output indicated for each sex.

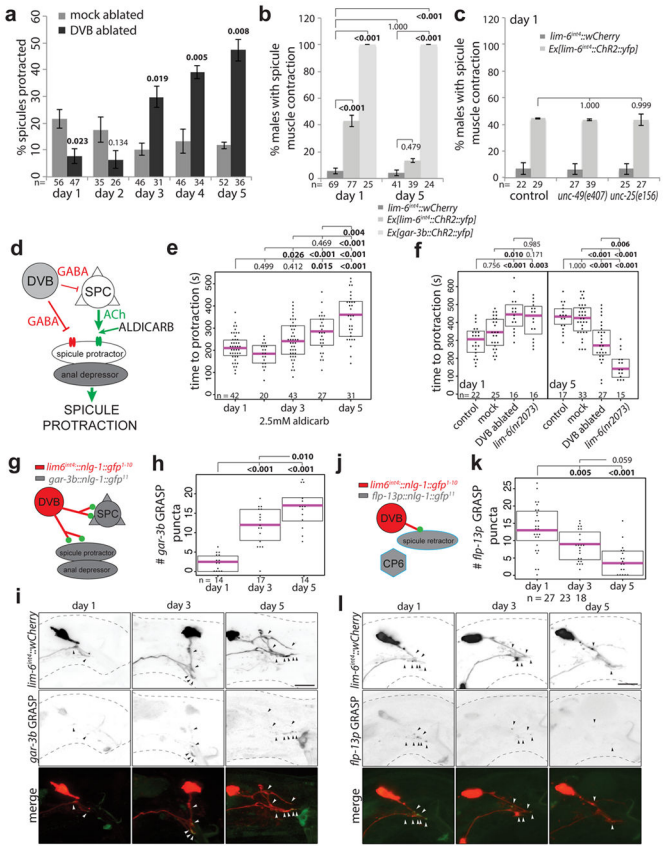

Fig. 2. DVB neuron undergoes a functional switch in adulthood resulting in dynamic behavioral output

(a) Percent of mock or DVB-ablated males with chronically protracted spicules 20 hours after ablation at day indicated (mean +/− S.E.M., two-tailed Student's t-test). **(b)** Percent of worms responding to 488nm light with movement of spicules for control, Ex[*lim-6*^{int4}*::ChR2::yfp]*, and Ex[*gar-3b::ChR2::yfp*](mean +/− S.E.M., one-way ANOVA and post-hoc Tukey HSD). **(c)** Percent of worms with or without Ex[*lim-6*^{int4}*::ChR2::yfp]* responding to blue light with spicule movement at day 1 in control, *unc-49(e407)*, and *unc-25(e156)* males (mean +/− S.E.M., one-way ANOVA and post-hoc Tukey HSD). **(d)** Diagram of GABA and acetylcholine input onto spicule muscles showing site of aldicarb action. **(e)** Males on 5mM aldicarb media timed for spicule protraction >5s (dot=one animal, magenta bar=median, and boxes=quartiles, one-way ANOVA and post-hoc Tukey HSD (true for f, h, and k)). **(f)** Control, mock-, DVB-ablated, or *lim-6(nr2073)* mutant males timed for aldicarb-induced spicule protraction 12 hours after ablation. **(g)** Diagram of *gar-3b* GRASP. **(h)** Quantification and **(i)** confocal images of *gar-3b* GRASP puncta. **(j)** Diagram of *flp-13p* GRASP. **(k)** Quantification and **(l)** confocal images of *flp-13p* GRASP puncta.

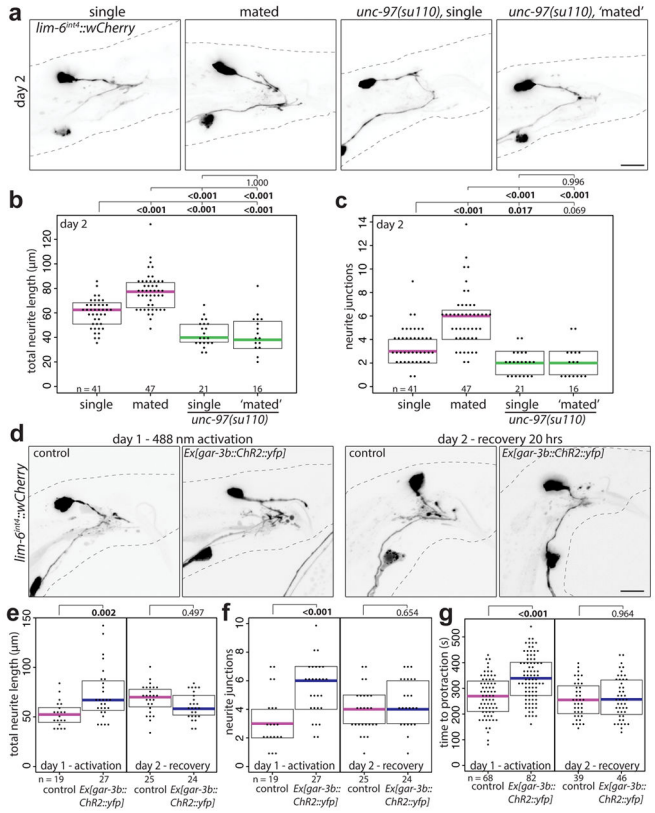

Fig. 3. DVB neurite outgrowth is experience-dependent, can be driven by circuit activity, and impacts behavior

(a) Confocal images of *lim-6*^{int4}*::wCherry*, **(b)** total neurite length, and **(c)** number or neurite junctions of males housed by themselves (single), with hermaphrodites (mated), *unc-97* mutant males housed by themselves (single), or with hermaphrodites ('mated') after 48h. Controls and males expressing channelrhodopsin (Ex[*gar-3b::ChR2::yfp*]) activated at day 1 (488 nm light for 3×15s every 45 mins for 4.5h) or recovered for 20h (day 2). **(d)** Confocal images of DVB (*lim-6*^{int4}*::wCherry*), and quantification of **(e)** total neurite outgrowth, **(f)** number of neurite junctions, and **(g)** time to spicule protraction on aldicarb. (dot=one animal, magenta bar=median, and boxes=quartiles, one-way ANOVA and post-hoc Tukey HSD).

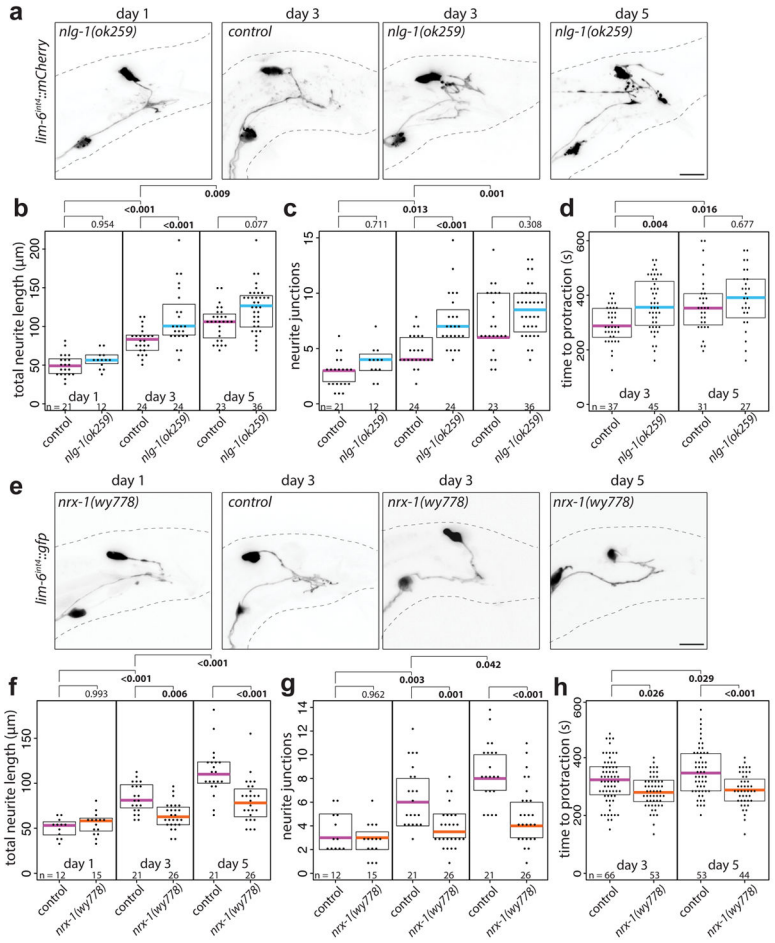

Fig. 4. Neuroligin and neurexin impact DVB neurite outgrowth and spicule protraction behavior

(a) Confocal images of DVB (*lim-6*^{int4}*::wCherry)* in *nlg-1*(ok259) mutant and control and quantification of **(b)** total neurite outgrowth and **(c)** number of neurite junctions in *nlg-1*(ok259) and control. **(d)** Time to aldicarb-induced spicule protraction in control and *nlg-1*(ok259) males. **(e)** Confocal images of DVB (*lim-6*^{int4}*::gfp*) in *nrx-1*(wy778) mutant and control. Quantification of **(f)** total neurite outgrowth and **(g)** number of neurite junctions in *nrx-1*(wy778) and control. **(h)** Time to aldicarb-induced spicule protraction in control and *nrx-1*(wy778). (dot=one animal, magenta bar=median, and boxes=quartiles, one-way ANOVA and post-hoc Tukey HSD).